Combustion Theory and Modelling
Vol. 00, No. 00, July 2010, 1–13

Revised Manuscript

Applying Nonlinear Dynamic Theory to One-Dimensional Pulsating Detonations

Hamid Ait Abderrahmane, Frederick Paquet and Hoi Dick Ng *

Department of Mechanical and Industrial Engineering, Concordia University, Montréal, Québec, H3G 1M8 Canada

(*July 2010*)

The dynamical behaviour of one-dimensional pulsating detonations was investigated in detail, with the aid of nonlinear theory tools such as phase plots and correlation dimension. The period-doubling cascade, as routes to deterministic chaos, is depicted through the transformations of the attractors' shapes. Using a correlation dimension method, the dimension of the attractors is determined and we show that the chaos within an one-dimensional pulsating detonation is deterministic.

Keywords: detonation; nonlinear theory; chaos; one-dimensional; instability;

1. Introduction

Since the work on the Lorenz attractor [1] in 1963, finding and characterizing the routes leading to chaos have been the main focus of research in the field of nonlinear dynamics. Three universal routes to chaos have been identified: Feigenbaum, intermittency and quasi-periodic routes [2]. It is from this perspective that we investigate the problem of one-dimensional (1D) detonation instability, which has been the subject of extensive theoretical and numerical studies since the pioneering work of Erpenbeck [3], Fickett and Wood [4] and Lee and Stewart [5]. A detonation wave is a combustion-driven compression wave propagating at supersonic velocity. Its structure and propagation mechanism involve a strong coupling between the gas dynamics and chemical reactions [6]. The dynamics of real unsteady detonations is inherently nonlinear; therefore, it cannot be adequately described by linear analysis. In a simplified one-dimensional configuration, the nonlinear instability of an unsteady detonation manifests as periodic longitudinal pulsations of the self-propagating front. Recent advances in computational methods now permit high-resolution numerical simulations of idealized, 1D Chapman-Jouguet (CJ) detonations. Such simulations make it possible to examine the long-time evolution of the longitudinal instability and explore the nonlinear features far from the stability limit when a control parameter is varied [7-12]. The variation of the control parameter can cause the transition to chaos through a series of bifurcations which correspond to successive temporal symmetries breaking. As has been previously pointed out by several authors [e.g. 10, 13], such features of 1D pulsating

*Corresponding author. Email: hoing@encs.concordia.ca

ISSN: 1364-7830 print/ISSN 1741-3559 online

DOI: 10.1080/1364783YYxxxxxxxx
http://www.informaworld.com

detonation have a remarkable resemblance to those found in nonlinear dynamical oscillator.

To depict the nonlinear dynamics of the 1D pulsating detonations an extensive numerical investigation of 1D pulsating detonations has been carried out [e.g. 7, 9, 12, 14-15]. The activation energy, considered there as the control parameter, was varied and several time series patterns for the shock pressure were obtained. The analysis showed that the detonation becomes unstable when the activation energy is above a defined threshold. In that case the leading shock pressure exhibits oscillations at different modes. With the aid of power spectra and the bifurcation diagram the authors in [14] showed that, when the control parameter was systematically increased, the 1D Chapman-Jouguet (CJ) detonation undergoes a series of Feigenbaum bifurcations (i.e. period-doubling cascades) before its behaviour becomes chaotic. The authors also showed that a three-period oscillations window can be found within the chaotic range of the control parameter.

The analysis of the data in [14] was based on spectral methods (Fast Fourier Transform). However, these such methods lie on the framework of linear systems and thus, are not sufficiently adequate to handle intrinsic nonlinear behaviour. Although, in some cases, power spectra can furnish some useful preliminary information before trying to compute the quantitative characteristics of the observed dynamics, such as, dimensions, Lyapunov's spectrum, entropies, etc., the main fall-off of power spectra is the distinction between deterministic and stochastic chaos. A broadband power spectrum is not typical only of external noise (experimental or numerical), but it also occurs for complex nonlinear dissipative systems that exhibit low dimensional deterministic chaos. The distinction between deterministic and stochastic chaos is of primary importance and can be achieved by characterizing the dynamics of the system. In one case, when the system evolves nonperiodically and with impredictability on strange attractors that live in a phase space of finite dimension, the dynamics is called deterministic chaos. In other hand the dynamic is called stochastic chaos or noise when the dynamics of the system tends to occupy an arbitrarily large portion of the phase space. Furthermore, once a chaotic phenomenon is recognized, it is useful to give it some quantitative characterization. For example, the application of correlation dimension has become the most popular and widely used measure of the complexity on experimental strange attractors (see [16]).

To deepen the investigation of 1D pulsating detonations the numerical data (given in [14]) was revisited using the powerful nonlinear dynamics time series analysis to characterize the resulting attractors. The method applied relies upon the Takens embedding theorem and consists of the construction of phase portraits from the raw numerical data given in [14]. The method is described in detail before it is applied in section 3. The phase portraits for particular values of the control parameter were reconstructed and their particular correlation dimension were determined. The objective of this paper is to provide evidence that shall help in answering this question: Is there deterministic chaos in the one-dimensional pulsating detonation?

2. Problem formulation and numerical method

The unsteady nonlinear dynamics of the propagation of a one-dimensional detonation wave are modelled by solutions of the one-dimensional inviscid compressible, time-dependent reactive Euler equations. These are expressed as the conservation equations for mass, momentum and energy together with a single-step irreversible Arrhenius kinetic rate law. In conservative form, the governing equations are writ-

ten as:

$$\frac{\partial U}{\partial t} + \frac{\partial F\left(U\right)}{\partial x} = S\left(U\right) \tag{1}$$

where the conserved variable **U**, the convective flux **F** and the reactive source term **S** are, respectively,

$$U = \begin{pmatrix} \rho \\ \rho u \\ E \\ \rho\lambda \end{pmatrix} F(U) = \begin{pmatrix} \rho u \\ \rho u^2 + p \\ \left(E + p\right) u \\ \rho u \lambda \end{pmatrix} S(U) = \begin{pmatrix} 0 \\ 0 \\ 0 \\ \dot{\omega} \end{pmatrix} \tag{2}$$

with

$$\begin{aligned} E &= \tfrac{p}{(\gamma-1)} + \tfrac{\rho u^2}{2} + \rho\lambda Q \\ T &= \tfrac{p}{\rho} \\ \dot{\omega} &= -k\rho\lambda \exp\left(\tfrac{-E_a}{T}\right) \end{aligned} \tag{3}$$

where ρ, u, p, T and E are density, particle velocity, pressure, temperature and total energy per unit volume, respectively. λ is the reactive progress variable, which varies between 1 (for unburned reactant) and 0 (for product). The mixture is assumed to be ideal and calorically perfect (with constant specific heat ratio γ). The parameters Q and E_a represent the non-dimensional heat release and activation energy, respectively. These variables have been made dimensionless by reference to the uniform unburned state ahead of the detonation front.

$$\rho = \frac{\tilde{\rho}}{\tilde{\rho}_o}, p = \frac{\tilde{p}}{\tilde{p}_o}, T = \frac{\tilde{T}}{\tilde{T}_o}, u = \frac{\tilde{u}}{\sqrt{\tilde{R}\tilde{T}_o}}, Q = \frac{\tilde{Q}}{\tilde{R}\tilde{T}_o}, E_{\mathrm{a}} = \frac{\tilde{E}_a}{\tilde{R}\tilde{T}_o} \tag{4}$$

The pre-exponential factor k is an arbitrary parameter that merely defines the spatial and temporal scales. It is chosen such that the half-reaction zone length $L_{1/2}$, i.e. the distance required for half the reactant to be consumed in the steady Zel'dovich-von Neumann-Döring (ZND) wave, is scaled to unit length. Hence,

$$x = \frac{\tilde{x}}{\tilde{L}_{1/2}}, t = \tilde{t} \cdot \frac{\sqrt{\tilde{R}\tilde{T}_o}}{\tilde{L}_{1/2}}, k = \tilde{k} \cdot \frac{\tilde{L}_{1/2}}{\sqrt{\tilde{R}\tilde{T}_o}} \tag{5}$$

The computational setup follows previous studies by fixing the dimensionless parameters with the values $Q = 50$, $\gamma = 1.2$ while varying activation energy E_a as a control parameter so that detailed comparisons can be made with previously published results.

The reactive Euler equations with a single-step Arrhenius kinetics rate law as given by the above equations are solved using a hierarchical adaptive hydrodynamic code to simulate the inviscid, one-dimensional propagation of a detonation wave. The numerical method is based on a second-order centered TVD scheme following the MUSCL-Hancock approach [17]. The detailed description and validation of the method through several benchmark problems for detonation simulations can be found in [18]. An adaptive mesh refinement strategy, based on a hierarchical series of Cartesian grids, is adopted in the code to decrease mesh spacing in the regions

where higher resolution is needed [19]. For all the simulations, unless specified, an effective numerical resolution of 128 points per half-reaction zone length of the steady ZND detonation $L_{1/2}$ is used to ensure that the detailed features of the pulsating front are properly resolved. To describe the nonlinear dynamics of the 1D detonation, the data of single variable - the time evolution of the leading shock pressure or Von Neumann state pressure behind the 1D pulsating detonation wave obtained from numerical simulation of the Euler equations [14] - are used for the nonlinear dynamic analysis. Since the numerical scheme used to generate the raw data for time series analysis is a shock-capturing scheme, the state variable, i.e., the leading shock pressure of the pulsating detonation, is numerically identified using a small algorithm by first finding the maximum gradient in the flow field to locate the shock front and then checking at the few neighbourhood grid points for maximum pressure. Its detailed description and validation through several benchmark problems for detonation simulations can be found in [18]. It is also important to note that the procedure for the data analysis requires a constant time step while the time series originally obtained from the numerical simulations uses a variable time-step based on the CFL condition, (in this study, CFL Number = 0.80). Therefore, the raw data with the variable time steps were restructured into time series with constant sampling time $T_s = 0.1$ by standard interpolation procedure using MatLab.

3. Data analysis

3.1 Procedure

Using the procedure proposed by Packard et al. [20], a multi-dimensional phase portrait that tells much about the dynamical behavior of the system can be reconstructed from measurements or numerical calculation of single variable. This is typical of experimental situations where only a single variable (time series) is accessible for measurements, while the physical systems possess many essential degrees of freedom. The procedure relies on the reconstruction of the whole system's trajectory in an "*embedding space*" using the method of delay-time by Takens and Mañé [21]. Assume $x(t)$ to be one of n possible state variables which completely describes the dynamical process. $x(t)$ can be measured or numerically calculated at sampling time, T_s, and the resulting time series is written as:

$$\{x\left(t_0\right), x\left(t_0+T_s\right), x\left(t_o+2T_s\right) .....x\left(t_0+NT_s\right)\} \tag{6}$$

In general, n is unknown and $x(t)$ is the only measured information about the system. For dissipative systems the real trajectory lies on a d-dimensional attractor in phase space, where: $d \leq n$. Packard et al. [20] have shown that it is possible to "*embed*" the above time series in a m-dimensional embedding space and reconstruct a "*pseudo-trajectory*" through the following (embedding) vectors:

$$\begin{aligned}
&y_1 = \left(x\left(t_0\right), x\left(t_0+\tau\right), ...x\left(t_0+(m-1)\tau\right)\right)^T \\
&y_2 = \left(x\left(t_0+l\right), x\left(t_0+l+\tau\right)\right), ...x\left(t_0+l+(m-1)\tau\right)^T \\
&..... \\
&y_s = \left(x\left(t_0+(s-1)l\right), x\left(t_0+(s-1)l+\tau\right) .....x\left(t_0+(s-1)l+(m-1)\tau\right)\right)^T
\end{aligned} \tag{7}$$

Here τ is called "*delay-time*" or "*time lag*", and l is the sampling interval between the first components of adjacent vectors. $w = (m-1)\tau$ is the "*window length*" which

represents the time spanned by each embedding vector. A selection of appropriate values for the parameters m and τ in the embedding procedure is particularly crucial for the reliability of the results. To ensure equivalence between the topological properties of actual and reconstructed attractor, a formal criterion was proposed by Takens:

$$m \geq 2d + 1 \tag{8}$$

This criterion relates the embedding dimension, m, to the attractor dimension, d. It was shown that Taken's criterion is often too conservative. It is thus adequate to reconstruct the attractor in a space with a lower dimensionality. In practice, the dimension d of the attractor is unknown and it has to be determined. Moreover, for practical analysis involving experimental or numerical data, choosing optimum embedding parameter, m, and delay-time, τ, is more than not trivial but it needs to consider data accuracy and inherent noise within the data. For this reason, in this paper we adopted the interactive technique suggested by Albano et al. [22]. The authors have combined *a singular-value decomposition*, which leads to set of statistically independently variables, and the well-known *Grassberger-Procaccia algorithm* [16] to determine the dimension of the attractors. The detailed procedure is summarized below (see Appendix for an application):

- **Step 1:** First we choose m and τ so that the window $w = (m-1)\tau$ is few times the correlation time. The correlation time is the time of the decay of the autocorrelation between two trajectories of the system. The *autocorrelation function* is defined as:

$$g(t) = \frac{\sum_{k}^{N} \left(x(k\tau)\, x(k\tau + t)\right)}{\sum_{k}^{N} \left(x(k\tau)\right)^2} \tag{9}$$

  The one rule thumb for selecting a delay-time, τ, is to pick up the first zero-crossing of the *autocorrelation function*, or for a signal without regular oscillation, the time lag at which the *autocorrelation function* falls to about $\frac{1}{e} \approx 0.37$. The variation of this time lag is therefore not random; With this time lag the successive components of embedding vector that span the phase space become 'independent'.

- **Step 2:** Perform first a *singular decomposition* of the embedding matrix $\mathbf{Y}$ (Eq. 7). This consists on the decomposition of $\mathbf{Y}$ as $\mathbf{Y} = \mathbf{VSU^T}$ where $\mathbf{U^T}$ stands for matrix transpose of $\mathbf{U}$. $\mathbf{S}$ is the diagonal matrix. $\mathbf{V}$ is the matrix with orthogonal columns and $\mathbf{U}$ is the orthogonal matrix. The elements, $s(i)$, of the diagonal matrix $\mathbf{S}$ are known as *singular values*. Afterwards rotates the embedding matrix $\mathbf{Y}$ using the matrix $\mathbf{U}$.

- **Step 3:** The correlation dimension of the attractor can be determined using the Grassberger and Procaccia calculation in a sub-space of the rotated space spanned by the principal axis with singular values $s(i)$ exceeding 10^{-4}. The singular values below this threshold are considered to be originated from the existing noise. Note that the threshold of 10^{-4} is not an universal criterion; its value can be increased if the data contains high level of noise. In particular case where the dynamics is chaotic, the threshold should be more conservative (e.g.

a value of 10^{-3}) to avoid the contamination of the trajectories by the numerical noise. The Grassberger and Procaccia procedure consists first calculation, in an m-dimensional embedding space, the "*correlation integral*", defined as:

$$C_m(r) = \frac{1}{N_p} \sum_{|i,j|}^{N} \theta \left(r - \|y_i - y_j\| \right) \tag{10}$$

which is the fraction of the distances between embedding vectors that does not exceed r, called the threshold distance. This threshold is varied to estimate the correlation dimension. Here $\theta(.)$ is the usual Heaviside unit-step function. N_p is the number of the distance used in the sum. It is worth noting that the values of correlation integral with small r are sensible to the noise in the time-series while the values of correlation integral obtained at very large r are affected by the finite length of the time-series. Grassberger-Procaccia [16] show that the correlation dimension D_2, of the reconstructed attractors, is given by:

$$D_2 = \lim_{m \to \infty} \lim_{r \to 0} D_2 \left(m, r \right) \tag{11}$$

where $D_2(m, r)$ is the slope of the log-log plot of correlation integrals:

$$D_2 \left(m, r \right) = \frac{d \left[\log \left(C_m \right) \right]}{d \left[\log \left(r \right) \right]} \tag{12}$$

If the Taken's criterion is not satisfied, i.e., $m \leq 2D_2(m, r) + 1$, increase m until it does.

- **Step 4:** Vary the window $w = (m - 1)\tau$ to maximize the $log(r)$ interval where $log(C_m(r))$ is a straight line.

As discussed later, the dimension D_2 of the attractor is used to segregate between deterministic and stochastic chaos. When the correlation dimension, D_2, converges towards a constant value with the increase of the embedding dimension, m, the system is considered deterministic. The correlation dimension is considered as a lower bound of the number of state variables needed to describe the related dynamics. On the other hand, if the correlation dimension D_2 does not converge to a constant value but its value increases proportionally to the increase of embedding dimension, m, the system is considered as a stochastic process with an arbitrarily large number of degrees of freedom.

3.2 Application

As indicated above the parameter that controls the detonation is the activation energy. The analysis in [14] shows that there are critical values above which the system loses its stability or undergoes bifurcation. It is common to use a bifurcation diagram to identify the locations of these bifurcation values (see Fig. 1 obtained previously in [14]). A more detailed and resolved bifurcation diagram has also been constructed later in [15] using a higher order numerical scheme with shock fitting. From both the linear stability analysis and the numerical simulation, the critical value of the activation energy that defines the neutral stability boundary is found to be about 25.2. Above that, the steady ZND detonation loses its stability and becomes unstable. The instability manifests as a pulsating behaviour of the

detonation front; For example, for an activation energy of 27.0, the instability manifests as periodic oscillations (Fig. 2a). By applying the procedure described in previous section, the obtained attractor that depicts such bifurcation in phase space is the limit cycle shown in Fig. 2b. Increasing the value of the control parameter to 27.40, the system of equations that models this detonation has undergone a second Hopf bifurcation. The time series of the shock pressure exhibits a two-period oscillation (Fig. 3a); the corresponding attractor in phase plane is a double-limit cycle, shown in Fig. 3b. These two figures 3 show that for any given initial condition the system undergoes two oscillations before it comes back to it initial states. Increasing further the value of the control parameter to 27.8 and 27.82, the period-doubling bifurcation process repeats itself and yields attractors with four and eight cycles, respectively; see Figs. 4-5.

It is well established that a period doubling process such as the one described above might lead to chaos. Indeed, by increasing the value of the control parameter to 28 and 28.1, the phase plots show attractors which look weakly chaotic; (see Fig. 6-7b). Such attractors are well known in the nonlinear dynamics literature as "noisy limit cycles"; they arise after the saturation of doubling period cascades (see Bergé, Pomeau and Vidal [2]). These attractors are formed with 2^n disjoint periodic cycles. Within each of these cycles the dynamics is chaotic thus explaining why the cycles were called noisy. Increasing further the control parameter to 28.2, the attractor becomes a three-period cycle (see Fig.8b). According to nonlinear theory [2], this three-period cycle will undergo, similarly to the previous periodic cycles (Figs. 2-5), a cascade of period doubling periods that leads to chaos again. Hence, the three-period cycle attractor is a periodic window inserted within a chaotic region. As expected, increasing further the value of the control parameter to 28.3 the attractor becomes again chaotic. This time the corresponding attractor showed in Fig.9b exhibits more chaotic dynamics. Fig. 10 also shows the attractor that corresponds to the value of the control parameter equal to 30.

For feature comparison with experimental results, the geometrical characterization of the attractors is required. The correlation dimension has become the most widely used measure of the chaotic behavior or strange attractors. As defined above, the correlation dimension is the slope of the correlation functions and its value is already determined at **step 3** of the procedure described in the subsection above. The geometrical characterization of the attractors is summarized in Table 1. The dimension of the attractors is around one for the limit cycles in Figs. 2b-5b. The dimension of the attractors increases after the saturation of the double-period cascade to 2 and 2.93 respectively for the activation energies 28.0 and 28.1. These two high dimensions for the "noisy limit cycles" explain or confirm the presence of noise or chaotic dynamics within the limit cycles (Figs.6b-7b). After that the correlation dimension decreases towards one (three-period limit cycle) when the control parameter had been increased to 28.2; this confirms the existence of the periodic window in the bifurcation diagram [14]. Increase in correlation dimension which follows the augmentation of the control parameter E_a to 28.3 and 30.0 indicates that the three-period limit cycle has undergone another series of periodic doubling cascades that yield chaos (Note that the dimensions of the attractors in Figs. 9b-10b are not integer). Fig. 11 portrays the calculation of the correlation dimension from the correlation integral (see **step 3**) of the attractor in Fig. 10. This figure indicates that increasing the embedding dimension yields the curves of the correlation integral to converge towards a single curve; the slopes of their linear parts also converge to a single value. The slope of the linear part of these curves which is the largest possible (**step 4**), is by definition the correlation dimension, D_2 or simply the dimension, d of the attractor. The convergence of the correlation

dimension towards a non-integer constant value of 2.84 at high value of the control parameter $E_a = 30.0$, (Fig. 11) indicates that the dynamics of the detonation is deterministic chaos, and not stochastic.

To look at the influence of numerical resolution on the correlation dimension results, Table 2 shows the estimate correlation dimensions using time-series data obtained from the numerical computation with two grid resolutions, i.e., 128 and 256 points per half ZND reaction zone length $L_{1/2}$, for two activation energies values $E_a = 27.8$ and 30.0. It is worth noting that the correlation dimension values shown in this table do not vary much (less than 1%) when the grid resolution was further refined and this can thus confirm that the nonlinear dynamics is indeed due to the model behaviour and not to numerical artifacts.

Another important parameter worth to discuss is the sampling time frame (TF) (or length of the time series) used for the correlation dimension estimate, i.e. the amount of data points used in the algorithm. In all previous results displayed so far, a time frame of TF = 1200 was used for the periodic solution, which covers a significant number of oscillation cycles of the 1-D pulsating detonation wave dynamics. In all cases, only data after the computation had run for $t = 1000$ is considered and analyzed in order to remove any initial transient and allow the nonlinear dynamics to be 'saturated'. For the chaotic solution, a longer time frame of TF = 2500 was used. To investigate if there is any effect of the time frame on the correlation dimension results, Table 3 shows the calculated results using three different sizes of time frame for the $E_a = 30.0$ case with 256 points grid resolution. As noted in the table, the small discrepancy can be due to inherent numerical errors in the algorithm used for the dimension estimate. Nevertheless, the difference is not more than 1% with a wide range of time frame, which is generally considered good for this type of time-series analysis as done in other fields of physics [24].

4. Concluding remarks

Detonation waves are inherently nonlinear. Theories and methodologies developed in nonlinear dynamics can provide another way to explore the rich nonlinear behaviour and characteristics behind the unstable detonation phenomena. In this paper, a detailed nonlinear dynamic analysis on the time series computed using numerical simulations of the one-dimensional inviscid compressible reactive Euler equation with single step Arrhenius kinetics was performed to model the propagation of an unsteady detonation wave. The results are tested for evidence of chaotic dynamics using concepts and techniques of nonlinear dynamics commonly applied to time series.

The dynamics and nonlinear characteristics of one-dimension pulsating detonation are depicted using phase portraits and correlation dimensions. The attractors of the system were reconstructed using the embedding or time delay method. The analysis shows conclusively that the resulting chaos following the period-doubling is deterministic, which the previous analysis using Fast Fourier Transform fails to characterize. The fact that the dynamics of the detonation follows the universal route to chaos and the ensued chaos is deterministic open possibilities for its feedback control as investigated in many other dynamical systems [25].

Acknowledgment This work is supported by the Natural Science and Engineering Research Council of Canada (NSERC).

References

[1] E.N. Lorenz *Deterministic nonperiodic flow*, J. Atmos. Sci. 20 (1963), pp. 130-141.
[2] P. Bergé, Y. Pomeau and C. Vidal, *Order Within Chaos*, Wiley, New York, 1986.
[3] J.J. Erpenbeck, *Stability of idealized one-reaction detonations*, Phys. Fluids 7 (1964), pp. 684-696.
[4] W. Fickett and W.W. Wood, *Flow calculations for pulsating one-dimensional detonations*, Phys. Fluids 9 (1966), pp. 903-916.
[5] H.I. Lee and D.S. Stewart, *Calculation of linear detonation instability: one-dimensional instability of planar detonations*, J. Fluid Mech. 216 (1990), pp. 103-132.
[6] J.H.S. Lee, *The Detonation Phenomenon*, Cambridge University Press, 2008.
[7] A. Bourlioux, A.J. Majda and V. Roytburd, *Theoretical and numerical structure for unstable one-dimensional detonations*, SIAM J. Appl. Math. 51 (1991), pp. 303-343.
[8] M. Short and J.J. Quirk, *On the nonlinear stability and detonability limit of a detonation wave for a model three-step chain-branching reaction*, J. Fluid Mech. 339 (1997), pp. 89-119.
[9] G.J. Sharpe, *Numerical simulations of pulsating detonations: I. Nonlinear stability of steady detonations*, Combust. Theory Modelling 4 (2000), pp. 557-574.
[10] G.J. Sharpe and S.A.E.G. Falle, *One-dimensional numerical simulations of idealized detonations.* Proc. R. Soc. London A 455 (1999), pp. 1203-1214.
[11] A.R. Kasimov, D.S. Stewart, *On the dynamics of self-sustained one-dimensional detonations: a numerical study in the shock-attached frame*, Phys. Fluids 16(10) (2004), pp. 3566-3578.
[12] L. He and J.H.S. Lee, *The dynamical limit of one-dimensional detonations*, Phys. Fluids 7(5) (1995), pp. 1151-1158.
[13] F. Zhang, R.S. Chue, J.H.S. Lee and R. Klein, *A nonlinear oscillator concept for one-dimensional pulsating detonations*, Shock Waves 8 (1998), pp. 351-359.
[14] H.D. Ng, A.J. Higgins, C.B. Kiyanda, M.I. Radulescu, J.H.S. Lee, K.R. Bates and N. Nikiforakis, *Nonlinear dynamics and chaos analysis of one-dimensional pulsating detonations*, Combust. Theory Modelling, 9 (2005), pp. 159-170.
[15] A.K. Henrick , T.D. Aslam , J.M. Powers, *Simulations of pulsating one-dimensional detonations with true fifth order accuracy*, J. Comp. Phys. 213 (2006), pp. 311-329.
[16] P. Grassberger and I. Procaccia, *Measuring the strangeness of strange attractors*, Physica D 9 (1983), pp. 189-208.
[17] E.F. Toro, *Riemann Solvers and Numerical Methods for Fluids Dynamics*, second ed., NewYork, Springer, 1999.
[18] H.D. Ng *The Effect of Chemical Reaction Kinetics on the Structure of Gaseous Detonations*, PhD thesis, McGill University, Montreal, Canada, 2005.
[19] M.J. Berger and J. Oliger, *Adaptive mesh refinement for hyperbolic partial differential equations*, J. Comp. Phys. 53 (1984), pp. 484-512.
[20] N.H. Packard, J.P. Crutchfield, J.D Farmer and R.S Shaw, *Geometry from a time series*, Phys Rev. Lett 45 (1980), pp. 712-716.
[21] F. Takens and R. Mañé, *Dynamical Systems and Turbulence*, Warwick, (1980); Lecture Notes in Mathematics, vol. 898, R. Rand and L.S. Young, ed., Springer, Berlin, 1981.
[22] A.M. Albano, J. Muench, C. Schwartz, A.I. Mees and P.E. Rap, *Singular-value decomposition and the Grassberger-Procaccia algorithm*, Phys Rev. A 38 (1988), pp. 3017-3026.
[23] P. Grassberger and I. Procaccia, *Dimensions and entropies of strange attractors from a fluctuating dynamics approach*, Physica D 13 (1984), pp. 34-54.
[24] J. Theiler, *Estimateing fractal dimension*, JOSA A 7 (1990), pp. 1055-1073.
[25] H.D. Abarbanel, *The analysis of observed chaotic data in physical system*, Rev. Mod. Phys. 65 (1993), pp. 1331-1392.

Appendix

In this appendix, the details of the time-series analysis are provided. To explain the method used in this paper, this appendix describes the basic steps of the nonlinear analysis algorithm by including figures and discussion. For illustration, the case for the activation energy $E_a = 30.0$ is discussed.

The first step in this algorithm procedure is to determine the delay-time τ. The one rule of thumb for choosing the delay-time is to pick up a first zero-crossing of the *autocorrelation function* $g(t)$ (see Eq. 9) when it features regular oscillations. When the function $g(t)$ does not feature regular oscillation, the delay-time is chosen at the first time when the value of $g(t)$ falls to $1/e \approx 0.37$.

For the case of activation energy $E_a = 30.0$, the correlation function does not exhibit regular oscillation and hence, the time-delay is picked up at the first time when the function $g(t)$ falls to $1/e \approx 0.37$; see Fig. A1. The correlation function falls down $1/e$ after the 30^{th} element; knowing that the sampling time is $T_s = 0.1$, the delay-time is then equal to $\tau = 3$.

In step 2, using the delay-time found in step 1 an embedding dimension, m, is chosen such that the window $w = (m-1)\tau$ is superior to the delay-time τ. As pointed out in Albano et al. [22], m should not be very high because higher embedding dimension m will include noises in the diagonal matrix $\mathbf{S}$ up to the level one can observe only noises. For this example, a reasonable choice lies between $m = 30$ and $m = 50$; a value $m = 30$ of is chosen here and the singular decomposition on the embedding matrix is then applied.

In step 3 the Grassberger and Procaccia calculation is applied in a sub-space spanned by the principal axes that corresponds to the singular values $s(i)$ of the matrix $\mathbf{S}$ exceeding 10^{-3}. The initial diagonal of the singular values which contains 30 elements will now contain only 25 elements; the fives are significantly small such that these are assumed to be originated from the numerical noises within the raw data. Having now the embedding dimension $m = 25$ and the delay-time from step 1, one can calculate the correlation dimensions for each embedding dimension; the result is presented in Fig. A2. The correlation dimensions for each embedding dimension which are the slopes of the linear part of the curves are also displayed in the following Fig. A3.

In step 4 the algorithm is to find the "good windows" $w = (m-1)\tau$ by varying the embedding dimension m. Using the delay-time and the embedding dimension $m = 25$, results of the step 1 and 3, respectively and analyzing the two figures above one can notice that the correlation dimension converges towards an asymptotic value with the increase of the embedding dimension. As observed in the Fig. A3 that for $m = 3$, there is a large interval $log(r)$ where $log(C_m(r))$ is a straight line. However, this embedding dimension does not satisfy Takens' criterion of $m \geq 2d+1$. Given the correlation dimension found in step 3, the embedding dimension $m = 7$ to $m = 25$ satisfies the Takens' criterion, giving also a relatively large $log(r)$ interval where $log(C_m(r))$ is a straight line; the correlation dimension approaches to the asymptotic value for m between $m = 17$ and $m = 23$. One can therefore consider any value from the interval $m = [17, 23]$ or the average correlation dimension within this interval. In this example case, the value of $m = 23$ is chosen. It is worth noting that varying the embedding dimension with few unites in the interval $m = [17, 23]$ will only result in a small effect on the value of the correlation dimension.

Table 1. Correlation dimensions for the attractors calculated using the Grassberger and Procaccia method [22,23].

Attractor (*figure number*)	D_2
Fig. 2	1.0087
Fig. 3	0.9910
Fig. 4	1.0153
Fig. 5	1.0343
Fig. 6	2.0004
Fig. 7	2.9317
Fig. 8	1.0466
Fig. 9	1.5953
Fig. 10	2.8404

Table 2. Correlation dimensions estimated for $E_a = 27.8$ and $E_a = 30.0$ using data obtained from two different grid resolutions.

	$E_a = 27.8$	$E_a = 30.0$
128 pts resolution	1.0153 ($m = 12$ and $\tau = 2.7$)	2.8404 ($m = 23$ and $\tau = 3$)
256 pts resolution	1.0109 ($m = 9$ and $\tau = 2.7$)	2.8557 ($m = 25$ and $\tau = 3$)

Table 3. The effect of time frame on the correlation dimension estimate for the case of $E_a = 30$ with results obtained using 256 points resolution.

Time frame TF	D_2	τ	m
2500	2.8557	3	25
4000	2.8746	2.9	25
5000	2.8680	2.9	24

Table caption

Table 1. Correlation dimensions for the attractors calculated using the Grassberger and Procaccia method [22,23].

Table 2. Correlation dimensions estimated for $E_a = 27.8$ and $E_a = 30.0$ using data obtained from two different grid resolutions.

Table 3. The effect of time frame on the correlation dimension estimate for the case of $E_a = 30.0$ with results obtained using 256 points resolution.

Figure caption

Fig. 1. Bifurcation diagram obtained in [14].

Fig. 2. Periodic oscillation and its corresponding limit cycle with $E_a = 27.0$, embedding dimension $m = 8$, time lag $\tau = 2.5$.

Fig. 3. 2- period oscillation and its corresponding double limit cycle with $E_a = 27.4$, embedding dimension $m = 13$, time lag $\tau = 2.5$.

Fig. 4. 4- period oscillation and its corresponding attractor with $E_a = 27.8$, embedding dimension $m = 12$, time lag $\tau = 2.7$.

Fig. 5. 8- period oscillation and its corresponding attractor with $E_a = 27.82$, embedding dimension $m = 15$, time lag $\tau = 2.7$.

Fig. 6. Attractor with $E_a = 28.0$, embedding dimension $m = 7$, time lag $\tau = 2.7$.

Fig. 7. Attractor with $E_a = 28.1$, embedding dimension $m = 9$, time lag $\tau = 2.8$.

Fig. 8. 3- period oscillation and its corresponding attractor with $E_a = 28.2$, embedding dimension $m = 20$, time lag $\tau = 2.2$.

Fig. 9. Chaotic oscillations and its corresponding attractor with $E_a = 28.3$, embedding dimension $m = 10$, time lag $\tau = 2$.

Fig. 10. Chaotic oscillations and its corresponding attractor with $E_a = 30.0$, embedding dimension $m = 23$, time lag $\tau = 3$.

Fig. 11. Correlation dimension of the strange attractor in Fig. 10. The slope $D_2 = 2.84$.

Fig. A1. Display of the autocorrelation function.

Fig. A2. Correlation dimension of the strange attractor for $E_a = 30.0$.

Fig. A3. Variation of the correlation dimension for different embedding dimension m.

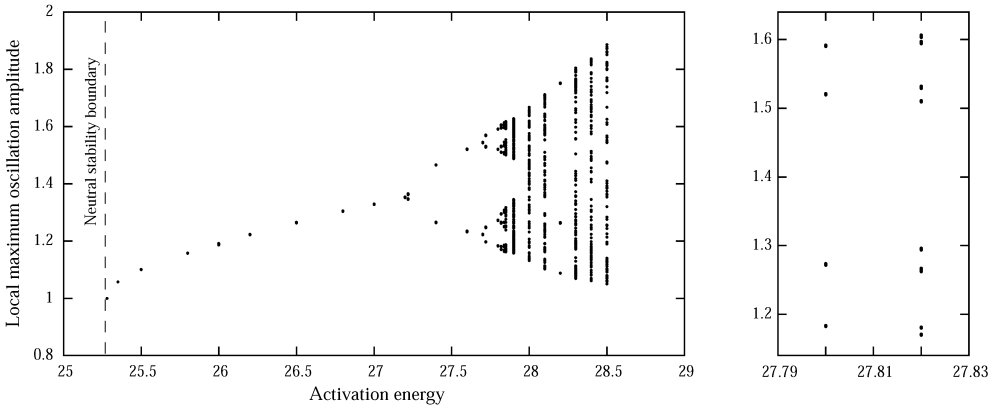

Figure 1. Bifurcation diagram obtained in [14].

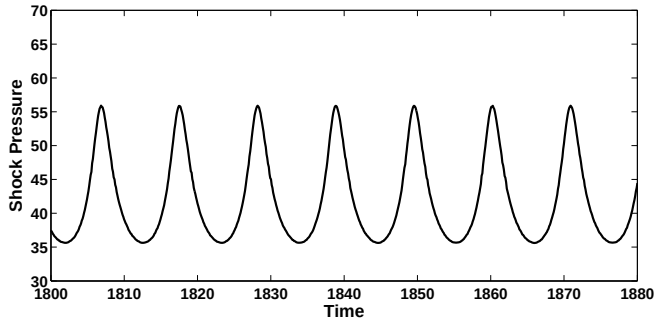

(a)

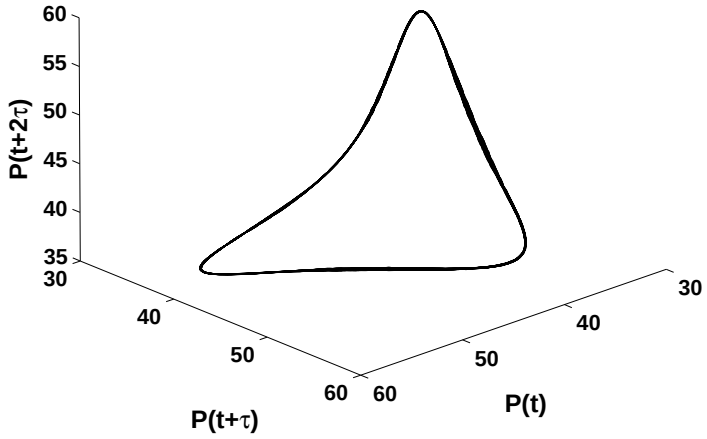

(b)

Figure 2. Periodic oscillation and its corresponding limit cycle with $E_a = 27$, embedding dimension $m = 8$, time lag $\tau = 2.5$.

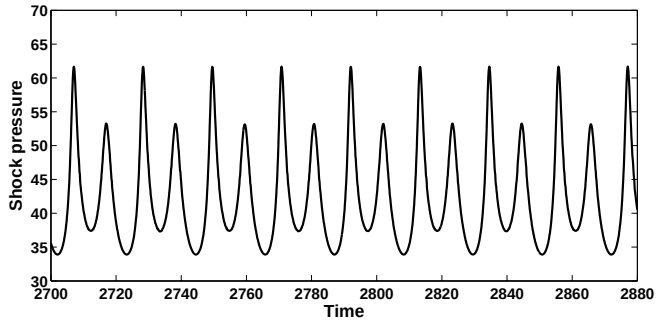

(a)

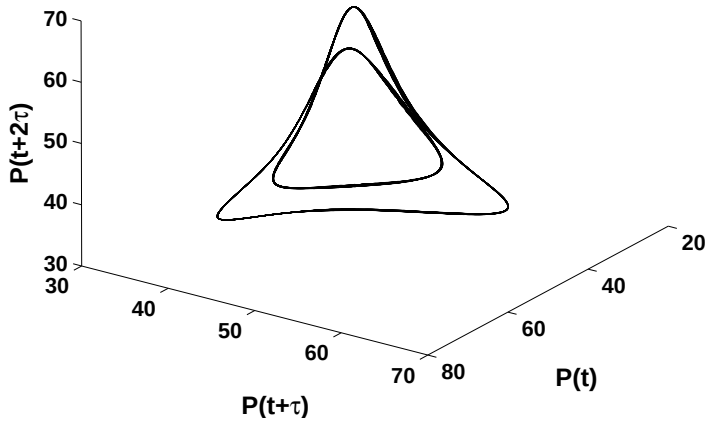

(b)

Figure 3. 2- period oscillation and its corresponding double limit cycle with $E_a = 27.4$, embedding dimension $m = 13$, time lag $\tau = 2.5$.

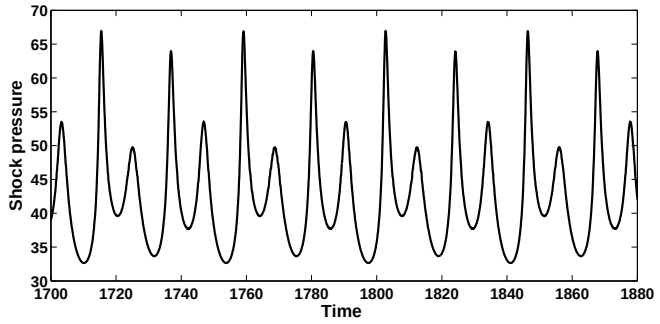

(a)

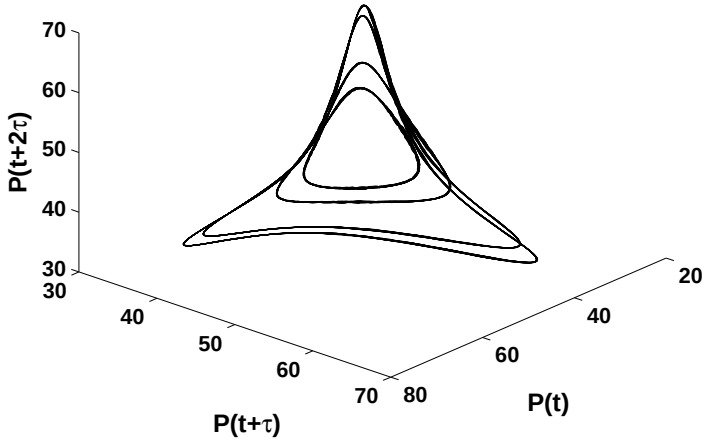

(b)

Figure 4. 4- period oscillation and its corresponding attractor with $E_a = 27.8$, embedding dimension $m = 12$, time lag $\tau = 2.7$.

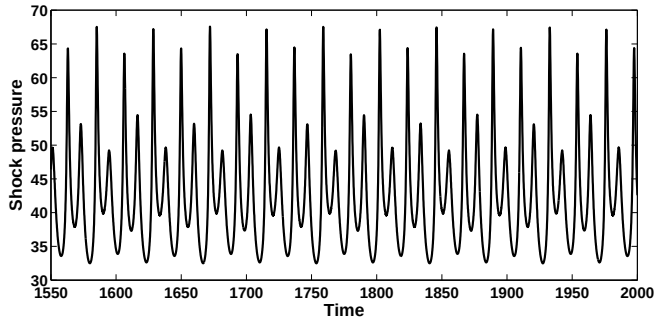

(a)

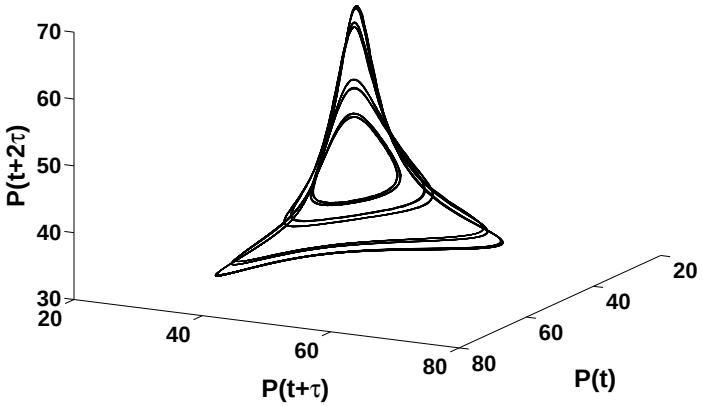

(b)

Figure 5. 8- period oscillation and its corresponding attractor with $E_a = 27.82$, embedding dimension $m = 15$, time lag $\tau = 2.7$.

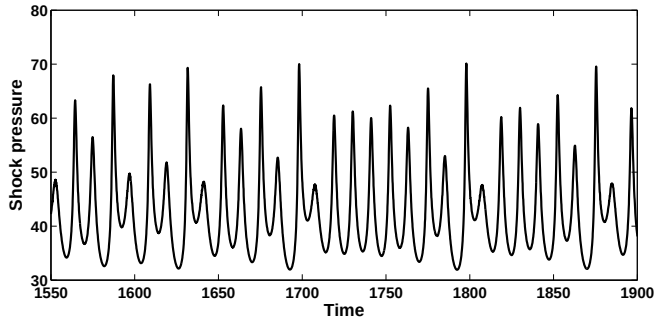

(a)

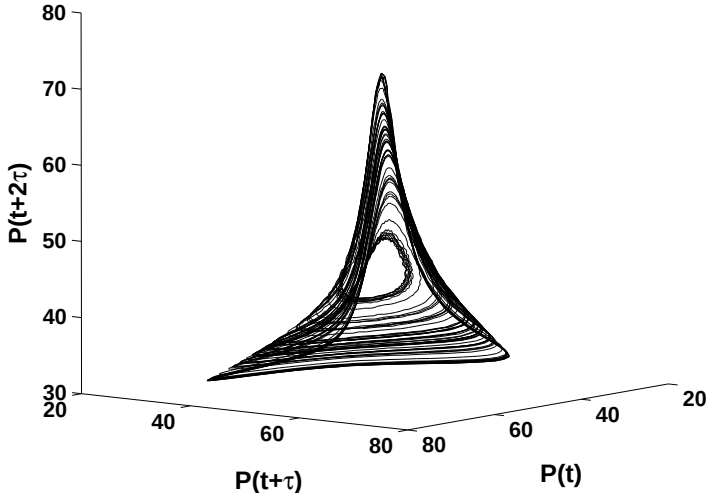

(b)

Figure 6. Attractor with $E_a = 28.0$, embedding dimension $m = 7$, time lag $\tau = 2.7$.

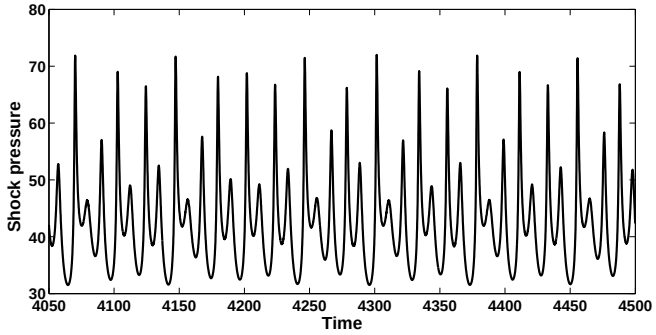

(a)

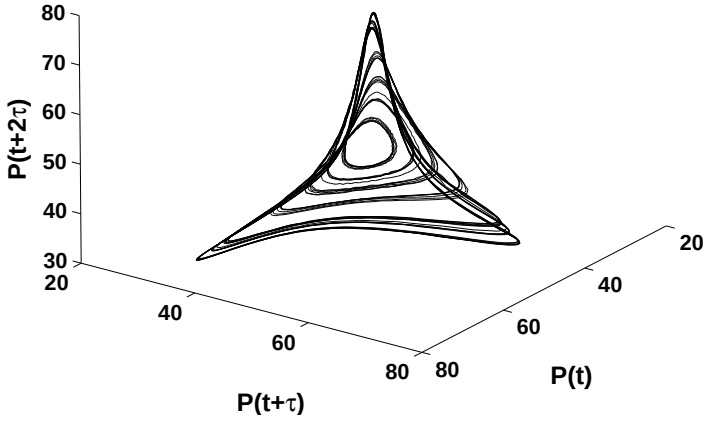

(b)

Figure 7. Attractor with $E_a = 28.1$, embedding dimension $m = 9$, time lag $\tau = 2.8$.

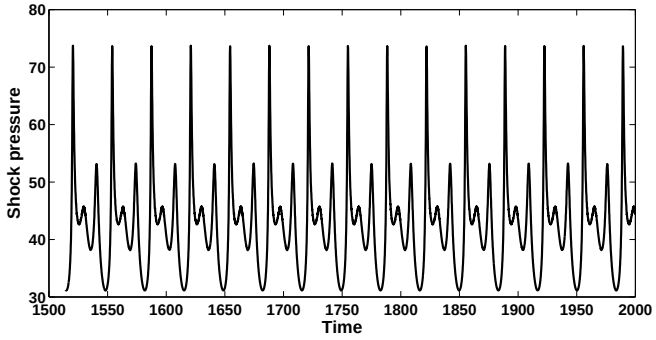

(a)

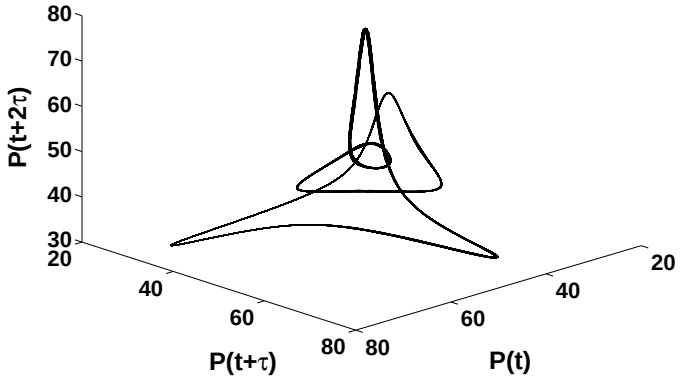

(b)

Figure 8. 3- period oscillation and its corresponding attractor with $E_a = 28.2$, embedding dimension $m = 20$, time lag $\tau = 2.2$.

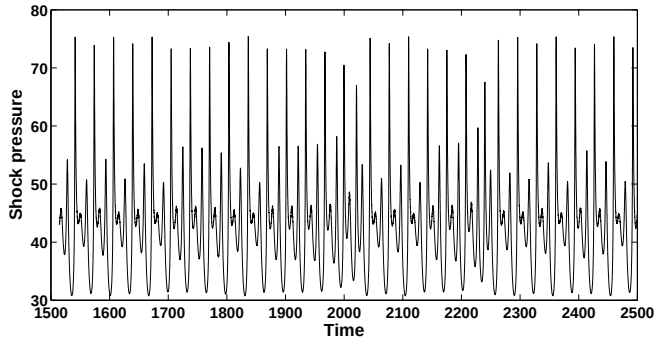

(a)

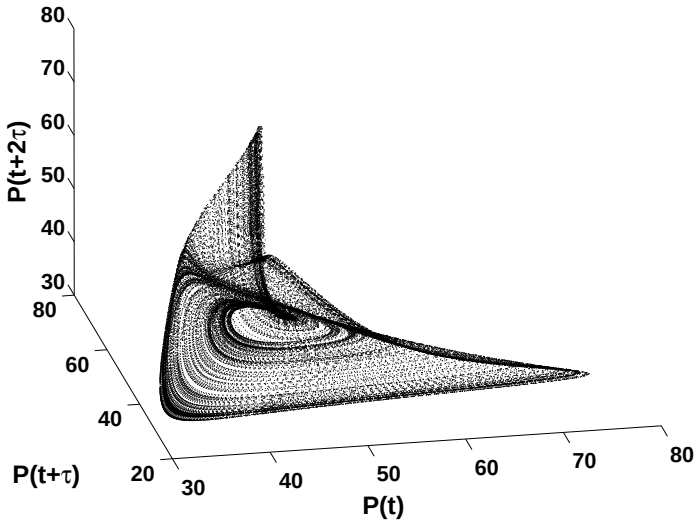

(b)

Figure 9. Chaotic oscillations and its corresponding attractor with $E_a = 28.3$, embedding dimension $m = 10$, time lag $\tau = 2$.

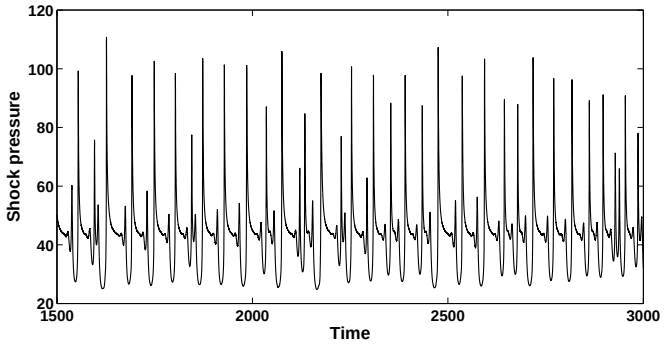

(a)

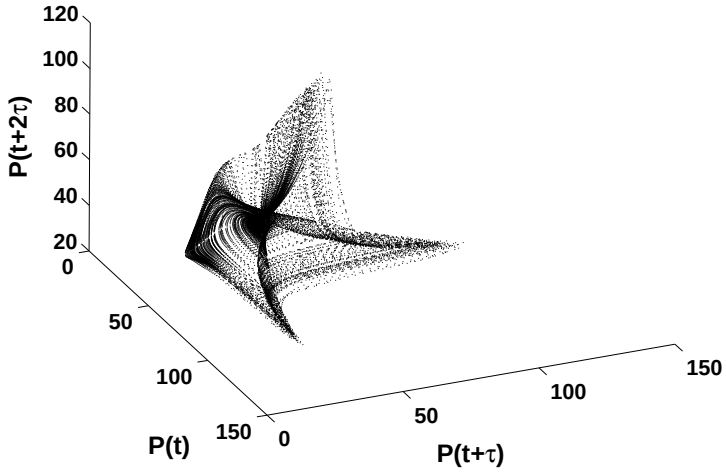

(b)

Figure 10. Chaotic oscillations and its corresponding attractor with $E_a = 30.0$, embedding dimension $m = 25$, time lag $\tau = 3$.

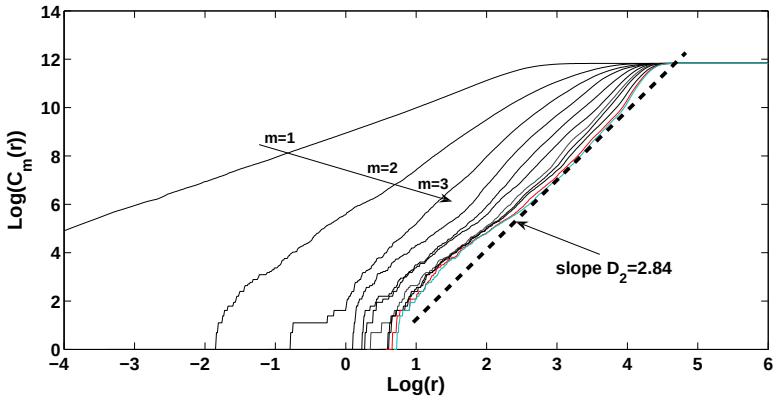

Figure 11. Correlation dimension of the strange attractor in Fig. 10. The slope $D_2 = 2.84$.

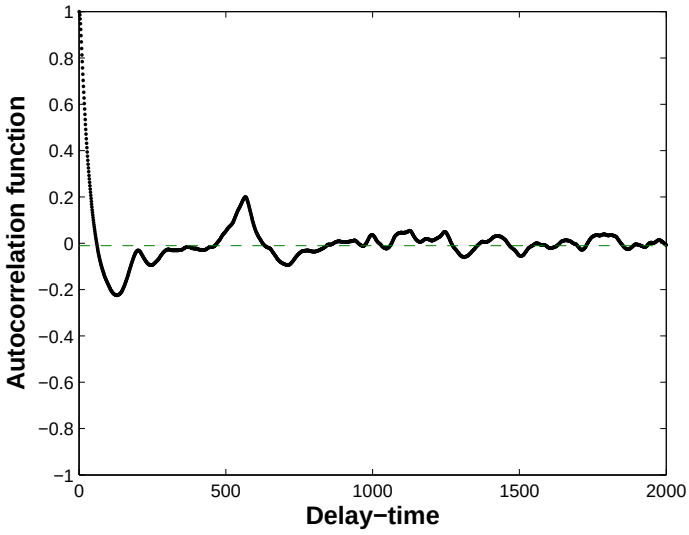

(a)

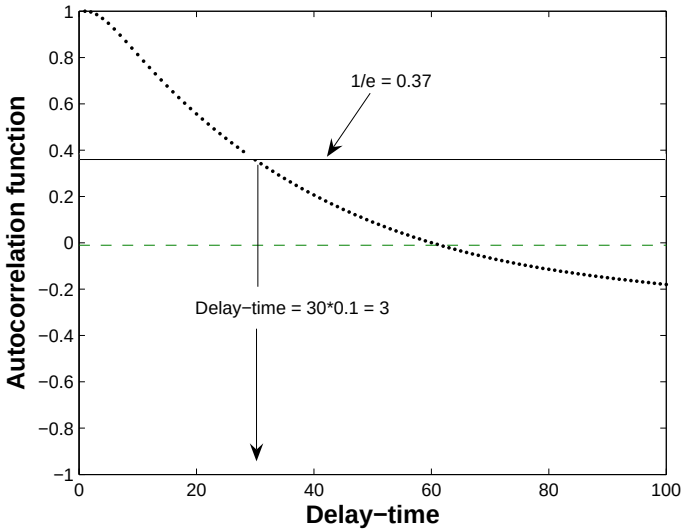

(b)

Figure 12. Display of the autocorrelation function.

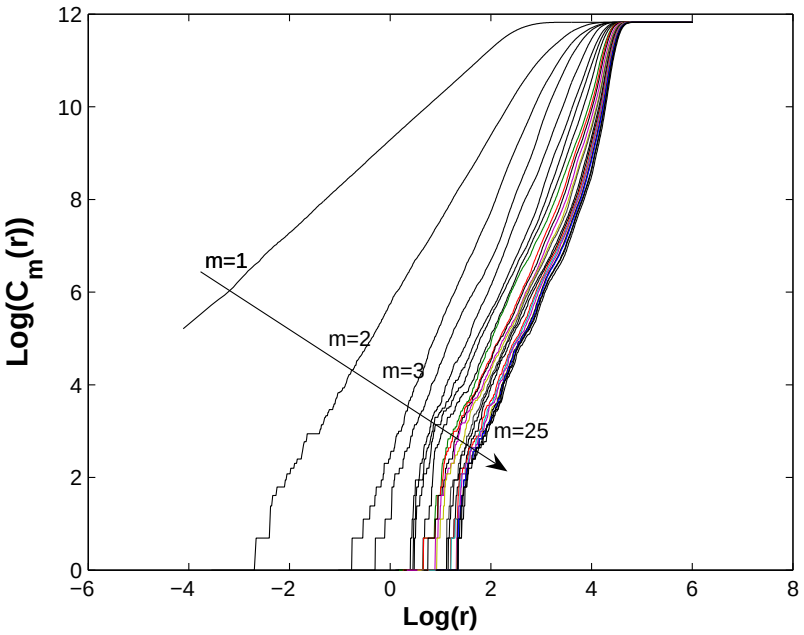

Figure 13. Correlation dimension of the strange attractor for $E_a = 30.0$.

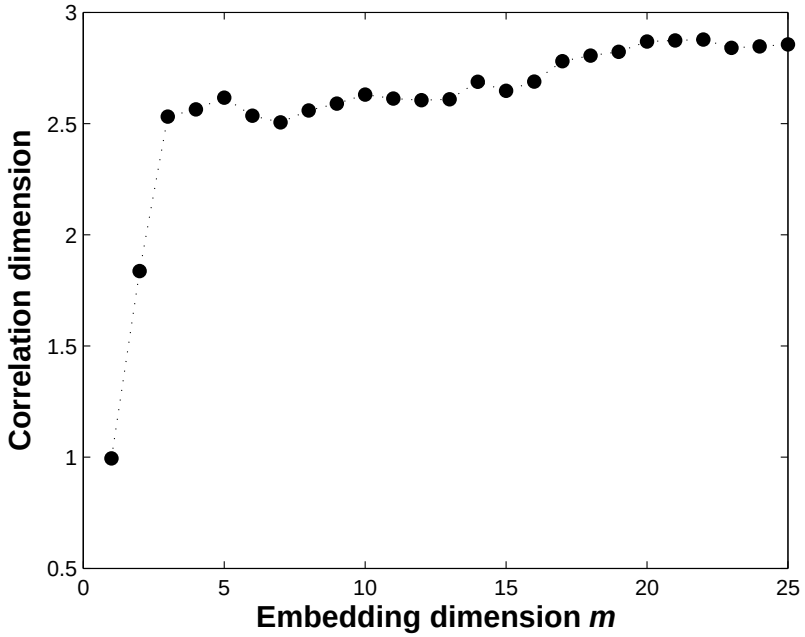

Figure 14. Variation of the correlation dimension for different embedding dimension m.